



This article appeared in a journal published by Elsevier. The attached copy is furnished to the author for internal non-commercial research and education use, including for instruction at the authors institution and sharing with colleagues.

Other uses, including reproduction and distribution, or selling or licensing copies, or posting to personal, institutional or third party websites are prohibited.

In most cases authors are permitted to post their version of the article (e.g. in Word or Tex form) to their personal website or institutional repository. Authors requiring further information regarding Elsevier's archiving and manuscript policies are encouraged to visit:

<http://www.elsevier.com/authorsrights>



Contents lists available at ScienceDirect

European Journal of Medicinal Chemistry

journal homepage: <http://www.elsevier.com/locate/ejmech>

Original article

Nonclassical antifolates, part 5. Benzodiazepine analogs as a new class of DHFR inhibitors: Synthesis, antitumor testing and molecular modeling study[☆]Hussein I. El-Subbagh^{a,*}, Ghada S. Hassan^b, Shahenda M. El-Messery^c, Sarah T. Al-Rashood^d, Fatmah A.M. Al-Omary^d, Yasmin S. Abulfadl^e, Marwa I. Shabayek^e^a Department of Pharmaceutical Chemistry, Faculty of Pharmaceutical Sciences & Pharmaceutical Industries, Future University, 12311 Cairo, Egypt^b Department of Medicinal Chemistry, Faculty of Pharmacy, Mansoura University, P.O. Box 35516, Mansoura, Egypt^c Department of Pharmaceutical Organic Chemistry, Faculty of Pharmacy, Mansoura University, P.O. Box 35516, Mansoura, Egypt^d Department of Pharmaceutical Chemistry, College of Pharmacy, King Saud University, P.O. Box 2457, Riyadh 11451, Saudi Arabia^e Department of Pharmacology (Biochemistry Section), Faculty of Pharmaceutical Sciences & Pharmaceutical Industries, Future University, 12311 Cairo, Egypt

ARTICLE INFO

Article history:

Received 15 November 2013

Received in revised form

3 January 2014

Accepted 6 January 2014

Available online 13 January 2014

Keywords:

Synthesis

Tetrahydro-quinazolines

Dibenzo[b,e][1,4]diazepines

DHFR inhibition

Molecular modeling study

ABSTRACT

A new series of tetrahydro-quinazoline and tetrahydro-1*H*-dibenzo[b,e][1,4]diazepine analogs were synthesized and tested for their DHFR inhibition and *in vitro* antitumor activity. Compound **35** showed a remarkable DHFR inhibitory potency (IC₅₀, 0.004 μM) which is twenty fold more active than methotrexate (MTX). Compounds **17** and **23** proved to be fifteen fold more active than the known antitumor 5-FU, with MG-MID GI₅₀, TGI, and LC₅₀ values of 1.5, 46.8, 93.3 and 1.4, 17.4, 93.3 μM, respectively. Computer modeling studies allowed the identification that methoxy and methyl substituents, the π-system of the chalcone core, the nitrogen atoms, on the dibenzodiazepine ring as pharmacophoric features essential for activity. These mark points could be used as template model for further future optimization.

© 2014 Elsevier Masson SAS. All rights reserved.

1. Introduction

Dihydrofolate reductase (DHFR) is the key enzyme in folate metabolism; it plays a major role in the biosynthesis of nucleic acids through the catalysis of the NADPH reduction of 7,8-dihydrofolate to 5,6,7,8-tetrahydrofolate and intimately couples with thymidylate synthase for purine and pyrimidine production [1,2]. As a result, DHFR becomes an important target for anticancer and antimicrobial agents [3]. Pre-clinical and clinical studies identified a plethora of mechanisms of drug resistance that are the primary hindrance for the allocation of curative cancer chemotherapy. Drug discovery of novel antifolates with improved properties and superior activities remains an attractive strategy both in academic research and in the pharmaceutical industry [3,4]. Many quinazoline analogs are known to possess anticancer activity

through DHFR inhibition as non-classical antifolates such as trimetrexate (TMQ) and piritrexim (PTX), Chart 1 [5–11]. On the other hand, benzodiazepine derivatives have been reported to possess antiviral, antimicrobial, and antitumor activities [12]. Meanwhile, the α,β-unsaturated ketone function condensed with variety of cyclizing agents such as hydrazine hydrate, thiourea, malononitrile, ethylcyanoacetate, and 2-aminothiazoles produced compounds possessing broad spectrum antineoplastic activity against variety of tumor cell lines [13–18].

Recently, a new series of substituted-quinazolin-4-ones was designed, synthesized, and evaluated for their *in vitro* DHFR inhibition in our laboratories. This study allowed the allocation of active DHFR inhibitors with IC₅₀ values around 0.4 μM, bearing aromatic π-systems. Molecular modeling study of this class of compounds revealed the importance of the main pharmacophoric groups (the 4-carbonyl fragment, the basic nitrogen atom at N-1, and the hydrophobic π-system regions) as well as of their relative spatial distances in regard to the quinazoline nucleus. The substitution pattern and spatial considerations of the π-systems proved to be critical for DHFR inhibition [19–21].

[☆] For parts 1–4 see Refs. [19–22].

* Corresponding author. Tel./fax: +20 2 26186111.

E-mail address: subbagh@yahoo.com (H.I. El-Subbagh).

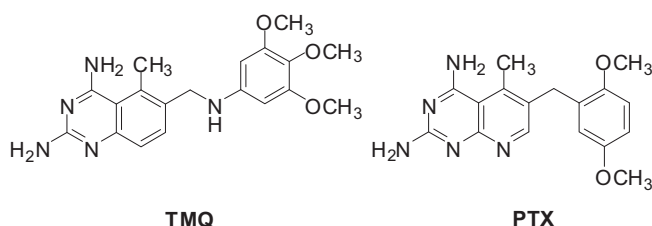


Chart 1. Structures of literature antifolate lead compounds.

In view of these facts, and in continuation to our previous efforts [19–28], the present study reports an efficient and reproducible synthesis of new series of tetrahydroquinazoline and tetrahydro-1*H*-dibenzo[*b,e*][1,4]diazepine analogs accommodating α,β -unsaturated imine function (the isosteric analog of the α,β -unsaturated ketone) in their structures. Those moieties are known to contribute to the anticancer activity [13–18]. Structure modifications of the quinazoline nucleus through its partial saturation into tetrahydroquinazoline or ring expansion into benzodiazepine have been performed to define the structure requirements and features that enhance selectivity and specificity for the tight binding to DHFR active site. The aim of this study is to identify novel synthetic lead compound(s) tackling the folate pathway. Compounds possessing DHFR inhibition activity might be suitable candidates for treating cancer. The new synthesized derivatives were tested for their *in vitro* DHFR inhibition and *in vitro* antitumor activity using the NCI's disease-oriented human cell lines assay [29–32].

2. Results and discussion

2.1. Chemistry

The synthetic strategy to prepare the target compounds is depicted in Scheme 1. The reported intermediate compounds (2*E*,6*E*)-2,6-dibenzylidenecyclohexanone derivatives **7–11** [18] were prepared by the reaction of cyclohexanone (**1**) with variety of substituted benzaldehydes such as 4-bromo- (**2**), 4-chloro- (**3**), 4-methoxy (**4**), 3,4-dimethoxy- (**5**), 3,4,5-trimethoxy-benzaldehyde (**6**) in ethanolic solution of sodium hydroxide. The target compounds 2-methyl-tetrahydroquinazolines (**13–17**) were obtained in considerable yields by reacting the α,β -unsaturated ketones **7–11** with acetamidine HCl (**12**). Similarly, the reported 2-amino-tetrahydroquinazolines **19–23** were synthesized by reacting **7–11** with guanidine HCl (**18**). Unlike earlier reports for the synthesis of 2-aminopyrimidines from chalcones and guanidine hydrochloride where an oxidizing agent is required to convert dihydropyrimidines to pyrimidines, in the present study the aromatization took place spontaneously with simple aerial oxidation [33]. The reaction mechanism suggested to get the target compounds involves Michael addition of either acetamidine (**12**), guanidine (**18**), or phenylenediamines (**24–26**) on one of the two olefinic bonds of enone moiety (**7–11**) to give an intermediate followed by reaction between the amine group and the keto group of enone to give the cyclic products, upon dehydration the dihydropyrimidine skeleton is formed. The latter on tautomerization aromatizes itself by the aerial oxidation to give finally the target compounds. On the other hand, the target compounds dibenzo[*b,e*][1,4]diazepines (**27–31**), 7,8-dimethyl-dibenzo[*b,e*][1,4]diazepines (**32–36**), and 7,8-dichloro-dibenzo[*b,e*][1,4]diazepines (**37–41**) were synthesized by reacting **7–11** with the appropriate substituted phenylenediamines **24–26** in glacial acetic acid (Scheme 1, Table 1).

All compounds were purified by recrystallization and were characterized on the basis of their spectroscopic (^1H NMR, ^{13}C NMR

and Mass spectrometry) data and microanalyses. Starting with the ^1H NMR spectra of 2-methylpyrimidines derivatives **13–17**, proton singlets of CH_3 group were observed at around 1.21–1.25 ppm. The only olefinic proton, $\text{CH}=\text{C}$ appeared as a singlet in the range of δ 7.57–7.60 ppm. The alicyclic and aromatic protons were observed at their usual chemical shifts. On the other hand, the ^1H NMR spectra of dibenzodiazepine analogs **27–31** showed the appearance of broad peak for NH group observed at 6.65–6.76 ppm. This peak is characteristic to the other analogs **32–41**, in addition to the appearance of singlet that refers to the 2 CH_3 group of **32–36** at 1.68–1.86 ppm. Elemental microanalysis, in conjunction with MS confirmed and further differentiated the incorporation of either halogens such as **27** or methoxy groups as **34**, along with the major protonated molecular ion peak at m/z 520 (9.4 M^+) and m/z 450 (11.2 M^+) respectively. ^{13}C NMR spectra were also in accordance to the depicted structures.

2.2. Dihydrofolate reductase (DHFR) inhibition

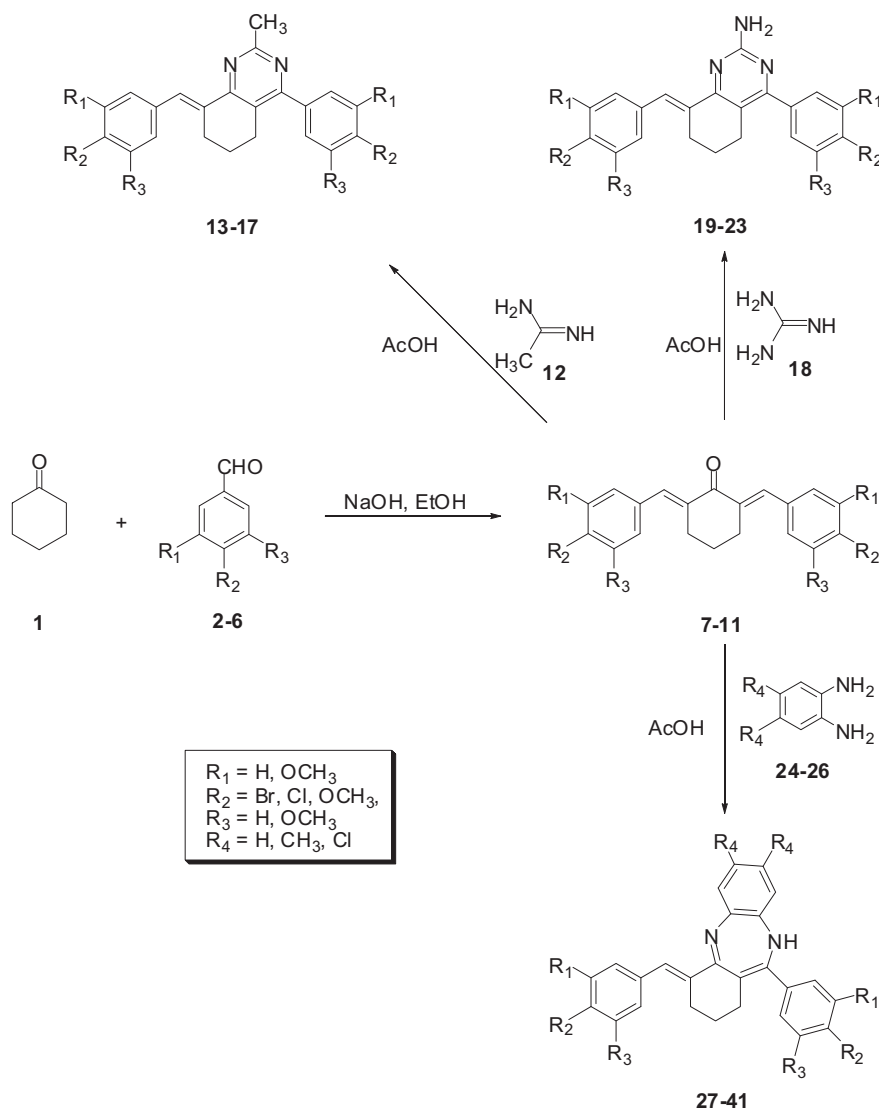
The synthesized compounds **7–41** were evaluated as inhibitors of bovine liver DHFR using reported procedures [34–36]. Results were reported as IC_{50} values (Table 1). Compound **35** showed a remarkable DHFR inhibitory potency (IC_{50} , 0.004 μM) which is twenty fold more active than methotrexate (MTX, IC_{50} , 0.08 μM) which used as a positive control. Compounds **30** and **31** proved to be almost equipotent to MTX activity with IC_{50} values of 0.06 and 0.09 μM , respectively (Fig. 1, Table 1). The rest of test compounds showed weak to moderate DHFR inhibition with IC_{50} values range of 0.1–21.0 μM .

2.3. *In vitro* antitumor screening

The synthesized compounds **7–41** were subjected to the National Cancer Institute (NCI) *in vitro* disease-oriented human cells screening panel assay for *in vitro* antitumor activity. A single dose (10 μM) of the test compounds were used in the full NCI 60 cell lines panel assay which includes nine tumor subpanels namely; Leukemia, Non-small cell lung, Colon, CNS, Melanoma, Ovarian, Renal, Prostate, and Breast cancer cells [29–32]. The data reported as mean-graph of the percent growth of the treated cells, and presented as percentage growth inhibition (GI %) caused by the test compounds (Table 2). Among the tested compounds, only compounds **13–17**, **19–23**, **28**, **29**, and **31** exhibited antitumor potency of various magnitudes.

Compounds **16**, **17**, **20**, **22**, **23**, **28**, and **31** showed remarkable broad spectrum antitumor potency and considered to be the most active members in this study. Meanwhile, compounds **13**, **14** and **15** displayed modest potency against the tested tumor cell lines and considered to be the least effective members. Concerning tumor cell line panel selectivity, compound **13** proved selective towards Leukemia, Colon, and Breast cancer panels while compound **15** exhibited selectivity towards Leukemia and Melanoma cancer panels. Regarding potency against individual cell lines, compound **14** proved lethal to Leukemia RPMI-8226 and Colon HCT-116 cancer cell lines; **19** proved lethal to Leukemia RPMI-8226, Colon HCT-116 and Melanoma LOX IMVI cancer cell lines; while **21** proved lethal to breast MDA-MB-468. Compound **19** showed 93.4 GI% towards Non-small cell lung cancer NCI-H522 cell line (Table 2).

The most active members of this study, compounds **16**, **17**, **20**, **22**, **23**, **28** and **31** passed the primary anticancer assay at an arbitrary concentration of 10 μM . Consequently, those active compounds were carried over and tested against a panel of 60 different tumor cell lines at a 5-log dose range [29–32]. Three response parameters, GI_{50} , TGI, and LC_{50} were monitored for each cell line, using the known drug 5-Fluorouracil (5-FU) as a positive control. Compounds



Scheme 1. Synthesis of the target compounds **13–17**, **19–23** and **27–41**.

17 and **23** proved to be fifteen fold more active than 5-FU, with MG-MID GI_{50} , TGI, and LC_{50} values of 1.5, 46.8, 93.3 and 1.4, 17.4, 93.3 μM , respectively; while compound **31** proved to be eleven fold more active than 5-FU, with MG-MID GI_{50} , TGI, and LC_{50} values of 2.0, 12.6, 61.7 μM , respectively (Fig. 1, Table 3).

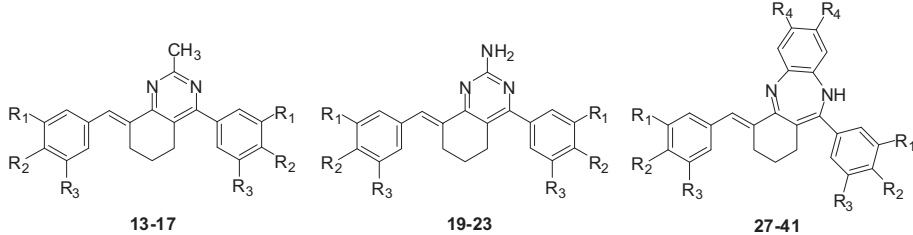
3. Structure–activity correlation

Two series of compounds were synthesized where structure modifications of the quinazoline nucleus was attained through its partial saturation into tetrahydroquinazoline (**13–17**, **19–23**) and ring expansion into dibenzo[*b,e*][1,4]diazepine (**27–31**, **32–36**, **37–41**) nuclei. Those alterations were performed to define the structure requirements and features that enhance selectivity and specificity for the tight binding to DHFR active site. It seems that the type of substituent attached to those two ring systems manipulate the biological activity. The 2-methyl-tetrahydroquinazoline analogs **16** and **17** with 8-(dimethoxy- or trimethoxy-benzylidene)- and 4-(dimethoxy- or trimethoxy-phenyl)-substituents showed DHFR inhibition potency with IC_{50} values of 0.1 and 0.5 μM , respectively. Replacement of the 2-methyl function of **16** and **17** by 2-amino

group produced compounds **19–23** with diminished DHFR inhibition activity with IC_{50} range of 14–21 μM . Ring expansion of **16** and **17** produced the dibenzo[*b,e*][1,4]diazepine derivatives **30** and **31** with remarkable DHFR inhibition potency of 0.06 and 0.09 μM , respectively.

In general, the electron withdrawing halogen atom did not contribute to the DHFR inhibition activity as evidenced by compounds **27** (IC_{50} 65.0 μM) and **33** (IC_{50} 70.0 μM). Meanwhile, the introduction of electron donating 4-methoxyphenyl function increased the potency as exemplified by compounds **29** (IC_{50} 0.6 μM) and **34** (IC_{50} 0.1 μM). It is proven that the introduction of dimethoxy function produced 3,4-dimethoxyphenyl and 3,4-dimethoxy-benzylidene analogs with a dramatic increase in the potency as shown in **30** (IC_{50} 0.06 μM) and **35** (IC_{50} 0.004 μM). Compound **35** is twenty fold more active than the DHFR inhibitor methotrexate (MTX, IC_{50} , 0.08 μM). The introduction of tri-methoxy group gave 3,4,5-trimethoxyphenyl and 3,4,5-trimethoxy-benzylidene derivatives with decreased activity as noticed in **31** and **36**.

Concerning the antitumor activity, electron donating methoxy function proved to contribute to the magnitude of potency rather than the electron withdrawing halogen atoms. Compounds **20** and

Table 1Physicochemical properties and DHFR inhibition activity results (IC₅₀, μ M) of the synthesized compounds **13–41**.


Compound	R ₁	R ₂	R ₃	R ₄	Yield, %	Mp, °C	Molecular formulae ^a	DHFR inhibition
13	H	Br	H	—	55	191–193	C ₂₂ H ₁₈ Br ₂ N ₂	nt
14	H	Cl	H	—	54	132–135	C ₂₂ H ₁₈ Cl ₂ N ₂	nt
15	H	OCH ₃	H	—	68	211–214	C ₂₄ H ₂₄ N ₂ O ₂	nt
16	OCH ₃	OCH ₃	H	—	64	176–178	C ₂₆ H ₂₈ N ₂ O ₄	0.1
17	OCH ₃	OCH ₃	OCH ₃	—	59	144–146	C ₂₈ H ₃₂ N ₂ O ₆	0.5
19	H	Br	H	—	48	207–209	C ₂₁ H ₁₇ Br ₂ N ₃	16.0
20	H	Cl	H	—	40	187–188	C ₂₁ H ₁₇ Cl ₂ N ₃	17.0
21	H	OCH ₃	H	—	32	227–229	C ₂₃ H ₂₃ N ₃ O ₂	18.0
22	OCH ₃	OCH ₃	H	—	52	204–206	C ₂₅ H ₂₇ N ₃ O ₄	14.0
23	OCH ₃	OCH ₃	OCH ₃	—	49	220–223	C ₂₇ H ₃₁ N ₃ O ₆	21.0
27	H	Br	H	H	81	112–115	C ₂₆ H ₂₀ Br ₂ N ₂	65.0
28	H	Cl	H	H	72	137–139	C ₂₆ H ₂₀ Cl ₂ N ₂	0.3
29	H	OCH ₃	H	H	43	188–190	C ₂₈ H ₂₆ N ₂ O ₂	0.6
30	OCH ₃	OCH ₃	H	H	51	158–160	C ₃₀ H ₃₀ N ₂ O ₄	0.06
31	OCH ₃	OCH ₃	OCH ₃	H	59	215–217	C ₃₂ H ₃₄ N ₂ O ₆	0.09
32	H	Br	H	CH ₃	62	133–135	C ₂₈ H ₂₄ Br ₂ N ₂	21.0
33	H	Cl	H	CH ₃	75	168–170	C ₂₈ H ₂₄ Cl ₂ N ₂	70.0
34	H	OCH ₃	H	CH ₃	66	184–186	C ₃₀ H ₃₀ N ₂ O ₂	0.1
35	OCH ₃	OCH ₃	H	CH ₃	44	140–142	C ₃₂ H ₃₄ N ₂ O ₄	0.004
36	OCH ₃	OCH ₃	OCH ₃	CH ₃	57	110–113	C ₃₄ H ₃₈ N ₂ O ₆	1.0
37	H	Br	H	Cl	50	177–179	C ₂₆ H ₁₈ Br ₂ Cl ₂ N ₂	0.1
38	H	Cl	H	Cl	75	154–156	C ₂₆ H ₁₈ Cl ₄ N ₂	12.0
39	H	OCH ₃	H	Cl	70	124–126	C ₂₈ H ₂₄ Cl ₂ N ₂ O ₂	nt
40	OCH ₃	OCH ₃	H	Cl	66	152–155	C ₃₀ H ₂₈ Cl ₂ N ₂ O ₄	nt
41	OCH ₃	OCH ₃	OCH ₃	Cl	61	162–164	C ₃₂ H ₃₂ Cl ₂ N ₂ O ₆	nt
Methotrexate	—	—	—	—	—	—	—	0.08

^a Compounds analyzed for C,H,N; results were within $\pm 0.4\%$ of the theoretical values for the formulae given. nt, not tested.

28 with 4-chlorophenyl substitution showed anticancer activity with MG-MID GI₅₀ values of 9.1 and 4.0 μ M, respectively. The introduction of tri-methoxyphenyl group produced compounds **17**, **23** and **31** with MG-MID GI₅₀ values of 1.5, 1.4 and, 2.0 μ M, respectively; which proved to be the most active antitumor members of this study.

It is worth mentioning that the active anticancer compounds **16**, **17**, **28** and **31** (MG-MID GI₅₀ 14.5, 1.5, 4.0, 2.0 μ M, respectively) seem to exert their antitumor activity through DHFR inhibition (IC₅₀ 0.1, 0.5, 0.3, 0.09 μ M, respectively). The other active anticancer compounds **20**, **22**, and **23** (MG-MID GI₅₀ 9.1, 5.2, 1.4 μ M, respectively) proved to be inactive DHFR inhibitors (IC₅₀ 17.0, 14.0, 21.0 μ M, respectively) which suggest that they might exert their antitumor activity through some other mechanism(s).

4. Molecular modeling study

The DHFR inhibitory activity of the new synthesized compounds **7–41** was experimentally determined. Compounds **30**, **31**, and **35** proved to be the most active members in the present study (IC₅₀, 0.06, 0.09 and 0.004 μ M, respectively) compared to the used positive control MTX (IC₅₀, 0.08 μ M). Compound **35** in particular, possessed extraordinary potency being twenty fold more active than MTX. Molecular modeling study was essentially needed to understand and interpret the unusual DHFR inhibitory pattern of this new class of compounds. It was interesting to start a

comparative modeling study of the most active DHFR inhibitor **35** and the least active compound **27** against MTX. The tertiary complex of human dihydrofolate reductase (hDHFR) crystal structure (pdb ID: 1DLS obtained from the protein data bank), NADPH and MTX were used as references for modeling and docking [37].

The binding of MTX to hDHFR is considered to be a complex interaction where hDHFR undergo isomerization and conformational changes resulting in tight binding to Glu30 [38–42]. The most active compound **35** and the inactive compound **27** were docked into the hDHFR binding site as a trial to explain their different destabilizing activity against DHFR assembly. The amino acid Lys46 is not one of the key residues involved in the recognition of the parent ligand MTX but it plays a critical role in the binding of the most active compound **35**. The 2D binding mode of **35** (IC₅₀ 0.004 μ M) docked and minimized in the hDHFR binding pocket was shown in Fig. 2a, b. Lys46 residue is linked to one of the methoxy groups of the side chain of **35** which suggest a similar interaction with the other active compounds **30**, **31** in addition to a hydrogen bonding network, this binding explains the diminished activity of **27** where the methoxy group is replaced by a bromine atom. This finding showed the necessity of such methoxy group for binding to hDHFR binding pocket. Compound **35** (IC₅₀ 0.004 μ M) and **27** (IC₅₀ 65.0 μ M) are similar in structure but significantly different in their hDHFR inhibitory activity, each compound has its own unique feature of binding profile. The most active **35** is located in and seems to be deeply buried inside the pocket site so it utilizes the

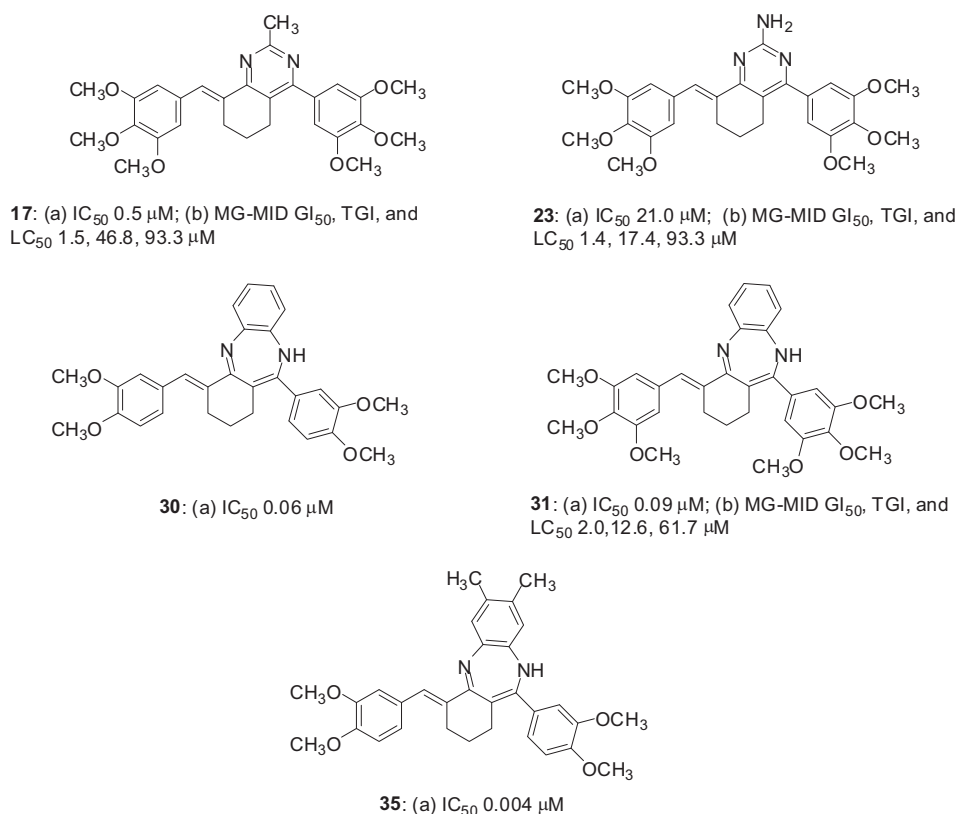


Fig. 1. Structures of (a) the active DHFR inhibitors **30**, **31** and **35** and (b) the active antitumor agents **17**, **23** and **31**.

pocket space efficiently. In the contrary, compound **27** seems to bind in a flipped fashion; one of the two 4-(4-bromo-benzylidene) moieties is placed into the pocket and the rest of the molecule is directed outwards from the active site (Fig. 3). Compounds **35** and **36** have a very similar structure and quite different DHFR inhibition activity. This could be explained through docking experiment which revealed that **36** and in contrary to **35**, could not bind to the active site of 1DLS through Lys46 leading to the loss of its activity. Furthermore, **36** binds in a flipped fashion directed outwards from the active site, similar to the binding mode of the least active compound **27**.

A comparative modeling study of both **35** and **27** against MTX was performed. Ligand-based active site alignment is a widely adopted technique for structure analysis of protein–ligand complexes. An approved alignment is acceptable when the molecules have similar shapes; aromatic moieties overlap; and low strain energy. The objective of computing a multiple ligand alignment for a set of input ligands is to maximize the similarity among ligands, while keeping their sound conformations. To probe similarity between the 3D structures of **35** and MTX, flexible alignment was performed. MOE/MMFF94 was employed to automatically generate superposition of the compounds under investigation with minimal user bias. 200 conformers of each compound were generated and minimized with a distance-dependant dielectric model. A low energy set of 100 was selected for further analysis [43,44]. Interestingly, compound **35** adopted nearly the same binding mode in a similar fashion as MTX (Fig. 4a), while **27** with its (4-bromophenyl)-tetrahydro-1H-dibenzodiazepine moiety seemed to adopt a different angle than that shown for MTX and could not reach as far into the enzyme pocket (Fig. 4b). Atomic-level details of the structure of pharmaceutically relevant receptors are not available; in such cases, 3D superposition of putative ligands can be used to

deduce specific structural requirements for biological activity [45,46]. Structure superposition of the active compounds **30**, **31** and **35** with their mark points such as methoxy substituents, the π -system of the chalcone core, N and NH atoms, methyl groups and the dibenzodiazepine ring are shown in Fig. 4c. The three compounds aligned fairly well, with almost complete superposition of the benzodiazepine rings (0.4 Å). This superposition suggests the possible existence of a region on the receptor suited for specific recognition of the aforementioned selected features. This hypothesis is consistent with the experimental data which strongly suggests that these mark points could be used as template model for further optimization.

Further investigation was conducted to explore the reasons behind the diminished DHFR inhibition activity of compound **27**, in comparison to **35**. Hydrophobic surface mapping study revealed that compounds bearing methoxy groups showed more lipophilic character than their bromo counterparts and hence were able to achieve more contact with the lipophobic pocket of the enzyme. In addition, compound **35**, pointed out more lipophilic regions attributed to the presence of two methyl groups (Fig. 5a). Moreover, **35** possess a more flat structure which allow the compound to adopt conformation that utilizes more hydrophobic space inside the pocket. On the other hand, the hydrophobic distributions of the least active compound **27**, showed less lipophilic moieties (no methoxy or methyl groups) and hence the required lipophilicity for effective binding to DHFR is diminished (Fig. 5b). Meanwhile, electrostatic potential isosurface maps of both compounds **35** and **27** were obtained. The two molecules showed different regions of high and low electrostatic potentials although of their structure resemblance. The electrostatic potential can be mapped onto the electron density surface by using color to represent the value of the potential. Colors toward green or blue represent positive potential

Table 2Percentage growth inhibition (GI%) of *in vitro* subpanel tumor cell lines at 10 μ M concentration of compounds **13–17**, **19–23**, **28**, **29**, **31**.

Tumor cell lines	% Growth inhibition (GI %) ^a												
	13	14	15	16	17	19	20	21	22	23	28	29	31
Leukemia													
CCRF-CEM	–	–	–	L	L	–	–	–	84.7	97.1	–	–	95.7
HL-60(TB)	–	–	–	L	L	–	35.2	32.2	57.7	L	–	–	98.5
K-562	–	–	–	94.1	88.9	–	56.5	–	44.0	93.6	52.8	49.1	94.7
MOLT-4	–	–	–	L	L	–	35.1	–	46.9	L	34.2	–	99.4
RPMI-8226	73.7	L	50.1	L	L	L	L	42.3	84.8	L	L	74.3	L
SR	–	–	–	–	–	54.1	79.2	–	71.9	99.0	78.5	46.1	97.3
Non-small cell lung cancer													
A549/ATCC	–	–	–	82.1	83.8	–	33.3	–	41.2	L	–	–	94.1
EKVX	–	–	–	–	–	–	–	–	–	44.0	–	–	40.2
HOP-62	–	–	–	67.9	78.0	–	–	–	43.0	82.2	–	–	L
HOP-92	–	–	–	69.9	–	–	–	31.4	–	L	39.4	–	–
NCI-H226	–	–	–	L	62.4	–	–	–	65.9	L	–	–	L
NCI-H23	–	–	–	70.9	66.1	–	38.9	–	50.7	88.4	–	–	91.5
NCI-322M	–	–	–	52.6	58.9	–	–	–	–	–	–	–	–
NCI-H460	–	–	–	99.4	L	–	–	–	35.4	L	–	–	L
NCI-H522	–	–	–	L	48.2	51.6	81.0	–	83.3	L	80.1	93.4	L
Colon cancer													
COLO 205	–	–	–	L	80.9	–	–	–	54.0	L	31.9	–	99.8
HCC-2998	–	58.5	–	L	88.1	51.5	L	–	–	L	–	–	L
HCT-116	55.8	L	–	L	L	L	L	–	92.1	L	L	61.9	L
HCT-15	–	–	–	L	95.8	–	41.7	–	64.1	L	36.4	–	93.9
HT29	–	45.6	–	L	92.1	67.8	92.3	–	75.8	L	84.1	–	L
KM12	–	62.0	–	93.8	97.1	53.0	97.7	–	67.9	L	82.7	72.5	L
SW-620	–	–	–	L	L	–	81.1	–	59.3	L	58.6	–	94.3
CNS cancer													
SF-268	–	–	–	80.0	78.8	–	–	–	36.2	84.9	–	–	74.0
SF-295	–	–	–	97.0	L	–	32.5	–	–	L	–	–	L
SF-539	–	–	–	82.9	86.5	–	–	–	–	74.1	–	–	64.9
SNB-19	–	–	–	39.6	38.8	–	–	–	–	38.5	–	–	35.6
SNB-75	–	–	–	64.8	78.1	–	–	–	36.1	54.3	–	–	45.5
U251	–	44.0	–	81.8	90.2	65.2	86.1	–	62.2	L	79.2	–	L
Melanoma													
LOX IMVI	–	63.2	–	L	L	L	L	–	87.1	L	L	42.6	L
MALME-3M	–	–	–	L	69.8	–	–	–	47.5	L	–	–	L
M14	–	34.7	–	L	L	38.1	89.0	–	42.7	L	70.9	–	L
MDA-MB-435	–	77.7	40.5	98.5	94.8	63.2	L	–	69.2	L	88.2	86.2	96.8
SK-MEL-2	–	–	–	94.1	73.4	–	–	–	43.2	L	–	–	82.1
SK-MEL-28	–	–	–	77.0	68.1	–	–	–	34.7	75.1	–	–	70.6
SK-MEL-5	–	–	–	93.8	80.9	–	–	43.8	60.3	L	–	–	L
UACC-257	–	–	–	79.8	56.2	–	–	–	53.8	L	–	–	83.8
UACC-62	–	–	–	89.1	91.0	–	–	32.1	47.2	L	–	32.0	L
Ovarian cancer													
IGORV1	–	–	–	75.6	69.3	–	–	–	42.9	L	–	–	L
OVCA-3	–	–	–	97.1	72.0	–	60.9	–	89.2	L	33.0	–	L
OVCA-4	–	–	–	79.1	57.8	–	–	–	46.7	73.1	–	–	66.5
OVCA-5	–	–	–	95.3	89.2	–	–	–	–	93.2	–	–	83.5
OVCA-8	–	–	–	96.9	94.1	–	58.8	–	89.4	L	34.3	–	81.4
NCI/ADR-RES	–	–	–	88.8	85.6	–	–	–	74.9	96.1	–	–	94.1
SK-OV-3	–	–	–	93.0	56.1	–	–	–	55.9	92.8	–	–	54.6
Renal cancer													
786-0	–	–	–	90.8	82.0	–	–	–	–	L	–	–	98.2
A498	–	–	–	94.1	83.7	–	45.3	–	–	99.5	32.8	–	L
ACHN	–	–	–	90.2	87.5	–	–	–	72.7	L	–	–	L
CAKI-1	–	–	–	94.9	88.6	–	–	–	44.2	L	–	–	93.5
RXF 393	–	–	–	L	77.4	–	65.5	–	79.1	L	34.7	–	L
SN12C	–	–	–	94.1	89.2	–	–	–	42.6	L	–	–	L
TK-10	–	–	–	87.8	55.5	–	–	–	–	–	–	–	–
UO-31	–	–	–	65.7	48.9	–	32.2	–	37.1	65.7	–	–	94.4
Prostate cancer													
PC-3	–	–	–	68.0	57.4	–	–	–	38.5	74.1	–	–	61.8
DU-145	–	–	–	92.7	95.1	–	–	–	–	L	–	–	95.1
Breast cancer													
MCF7	56.7	68.7	–	73.7	77.0	61.4	66.9	–	72.4	57.0	64.2	44.0	63.1
MDA-MB-231/ATCC	–	–	–	92.9	86.9	–	–	–	–	71.1	–	–	75.9
HS 578T	–	–	–	41.0	51.4	–	–	–	–	63.0	–	–	46.8
BT-549	–	34.0	–	L	97.1	–	–	–	63.9	L	–	–	L
T-47D	–	–	–	88.8	–	–	–	–	–	72.5	–	–	76.2
MDA-MB-468	–	–	–	L	L	–	37.8	L	L	L	40.0	56.4	L

^a GI < 30%; nt, not tested; L, compound proved lethal to the cancer cell line.

Table 3
Compounds **16**, **17**, **20**, **22**, **23**, **28**, **31** median growth inhibitory (GI₅₀, μ M), total growth inhibitory (TGI, μ M) and median lethal (LC₅₀, μ M) concentrations of *in vitro* subpanel tumor cell lines.

Compound	Activity	I	II	III	IV	V	VI	VII	VIII	IX	MG-MID ^a
16	GI ₅₀	6.8	37.8	28.9	34.2	26.9	25.5	23.7	26.9	15.7	14.5
	TGI	92.7	90.2	88.9	<i>b</i>	<i>b</i>	<i>b</i>	98.7	<i>b</i>	80.6	87.1
	LC ₅₀	<i>b</i>	<i>b</i>	<i>b</i>	<i>b</i>	<i>b</i>	<i>b</i>	96.9	<i>b</i>	99.2	<i>b</i>
17	GI ₅₀	1.1	2.7	0.9	34.5	1.4	1.9	2.2	1.8	2.6	1.5
	TGI	62.5	<i>b</i>	67.3	<i>b</i>	3.1	<i>b</i>	42.0	<i>b</i>	80.8	46.8
	LC ₅₀	<i>b</i>	<i>b</i>	76.2	<i>b</i>	<i>b</i>	<i>b</i>	<i>b</i>	<i>b</i>	<i>b</i>	93.3
20	GI ₅₀	7.8	15.2	4.0	13.7	15.4	16.0	14.7	12.3	23.6	9.1
	TGI	61.1	55.7	12.5	53.1	36.5	71.9	40.6	51.2	70.9	33.1
	LC ₅₀	<i>b</i>	88.6	51.3	91.9	80.0	94.1	78.4	95.0	92.2	72.5
22	GI ₅₀	2.1	22.1	17.4	26.7	5.5	19.6	7.8	5.1	3.9	5.2
	TGI	65.1	71.1	75.8	85.7	73.4	<i>b</i>	66.7	<i>b</i>	87.3	61.7
	LC ₅₀	<i>b</i>	94.3	89.8	<i>b</i>	95.6	<i>b</i>	93.6	<i>b</i>	<i>b</i>	95.5
23	GI ₅₀	1.3	1.7	1.1	3.3	1.3	1.9	1.8	2.7	2.0	1.4
	TGI	36.5	42.5	2.6	<i>b</i>	20.0	82.4	20.8	<i>b</i>	69.2	17.4
	LC ₅₀	<i>b</i>	<i>b</i>	68.3	<i>b</i>	<i>b</i>	<i>b</i>	<i>b</i>	<i>b</i>	<i>b</i>	93.3
28	GI ₅₀	4.1	9.0	2.4	4.9	9.5	4.3	3.3	5.1	4.6	4.0
	TGI	49.4	35.2	6.4	52.4	24.3	43.5	29.1	61.9	58.2	18.6
	LC ₅₀	<i>b</i>	81.3	38.8	84.3	64.2	93.8	64.0	<i>b</i>	88.1	56.2
31	GI ₅₀	1.4	2.8	1.6	6.8	1.7	2.6	2.3	2.3	2.9	2.0
	TGI	5.0	28.0	5.2	94.3	5.6	54.2	20.0	53.4	48.2	12.6
	LC ₅₀	<i>b</i>	73.6	36.4	<i>b</i>	71.4	<i>b</i>	68.4	<i>b</i>	89.4	61.7
5-FU	GI ₅₀	15.1	<i>b</i>	8.4	72.1	70.6	61.4	45.6	22.7	76.4	22.6
	TGI	<i>b</i>	<i>b</i>	<i>b</i>	<i>b</i>	<i>b</i>	<i>b</i>	<i>b</i>	<i>b</i>	<i>b</i>	<i>b</i>
	LC ₅₀	<i>b</i>	<i>b</i>	<i>b</i>	<i>b</i>	<i>b</i>	<i>b</i>	<i>b</i>	<i>b</i>	<i>b</i>	<i>b</i>

I, leukemia; II, non-small cell lung cancer; III, colon cancer; IV, CNS cancer; V, melanoma; VI, ovarian cancer; VII, renal cancer; VIII, prostate cancer; IX, breast cancer.

^a Full panel mean-graph midpoint (μ M).

^b Compounds showed values $>100 \mu$ M.

values, while colors toward red indicate less positive value of the electrostatic potential (Fig. 5c, d). It is pretty easy to distinguish that **35**, have more positive total charge density due to the presence of two methoxy groups, on the contrary to **27** which showed less positive total charge due to the absence of both methoxy and methyl groups (Fig. 5e, f), lacking of such hydrophobic moieties leading to diminished lipophilicity. The obtained charge distribution, electrostatic, hydrophobic mapping and conformations emphasize a distinct different interaction between the active and the inactive molecules with the potential protein-binding site and confirm the hypothesis that as the hydrophobicity of the molecule increases, the interaction to the DHFR binding site increases. The results of the computer modeling studies indicate striking differences in the mode of binding, hydrophobic, and electrostatic potential isosurface maps between the most active DHFR inhibitor **35**

versus the least active **27**, inspite of their structure similarity which in turn explain their different DHFR inhibition pattern.

5. Conclusion

Compounds **7–41** represent a new series of tetrahydroquinazoline and tetrahydro-1*H*-dibenzo[*b,e*][1,4]diazepine analogs bearing α,β -unsaturated imine function. Compound **35** showed a remarkable DHFR inhibitory potency (IC₅₀, 0.004 μ M) which is twenty fold more active than the DHFR inhibitor methotrexate (MTX). Compounds **17** and **23** proved to be fifteen fold more active than 5-FU, with MG-MID GI₅₀, TGI, and LC₅₀ values of 1.5, 46.8, 93.3 and 1.4, 17.4, 93.3 μ M, respectively; while compound **31**

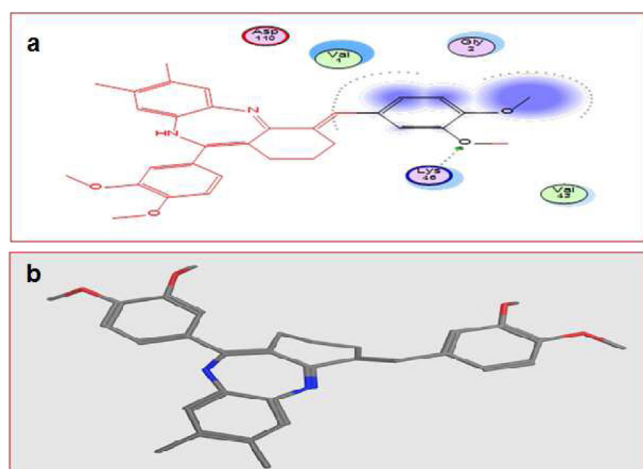


Fig. 2. (a) 2D binding mode and residues involved in the recognition for the most active compound **35** (IC₅₀ 0.004 μ M); (b) best docking pose for **35** docked and minimized in the hDHFR binding pocket.

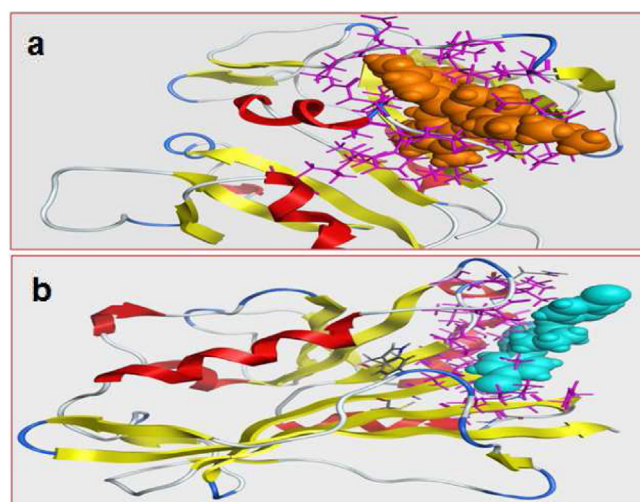


Fig. 3. (a) The aligned conformations of the most active compound **35** (IC₅₀ 0.004 μ M); (b) the most inactive compound **27** (IC₅₀ 65.0 μ M) exposing out of the pocket (cyan). (For interpretation of the references to color in this figure legend, the reader is referred to the web version of this article.)

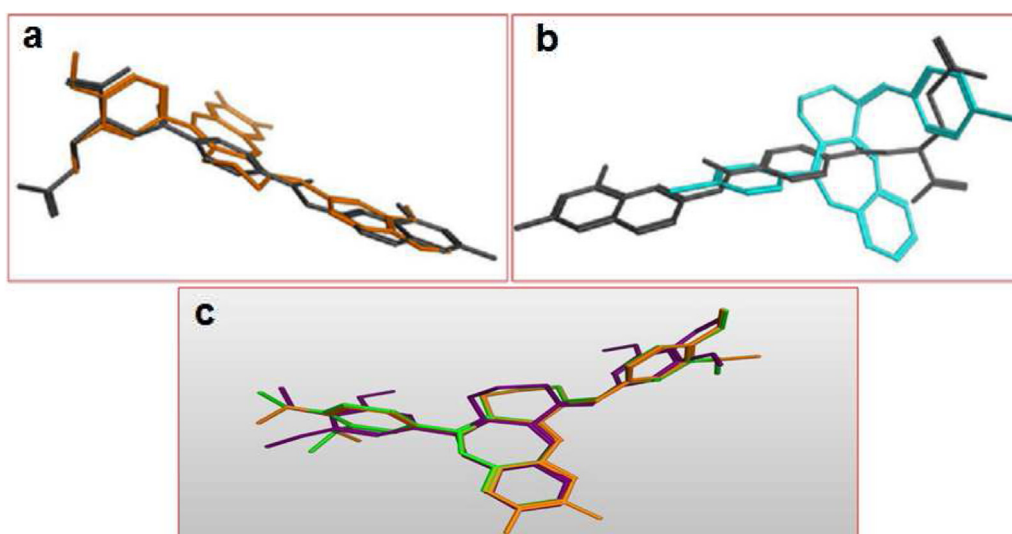


Fig. 4. (a) Flexible alignment of the most active compound **35** (orange) and MTX (gray); (b) the least active compound **27** (cyan), and MTX (gray) and (c) Superposition of the most active compounds **30** (green), **31** (violet) and **35** (orange). (For interpretation of the references to color in this figure legend, the reader is referred to the web version of this article.)

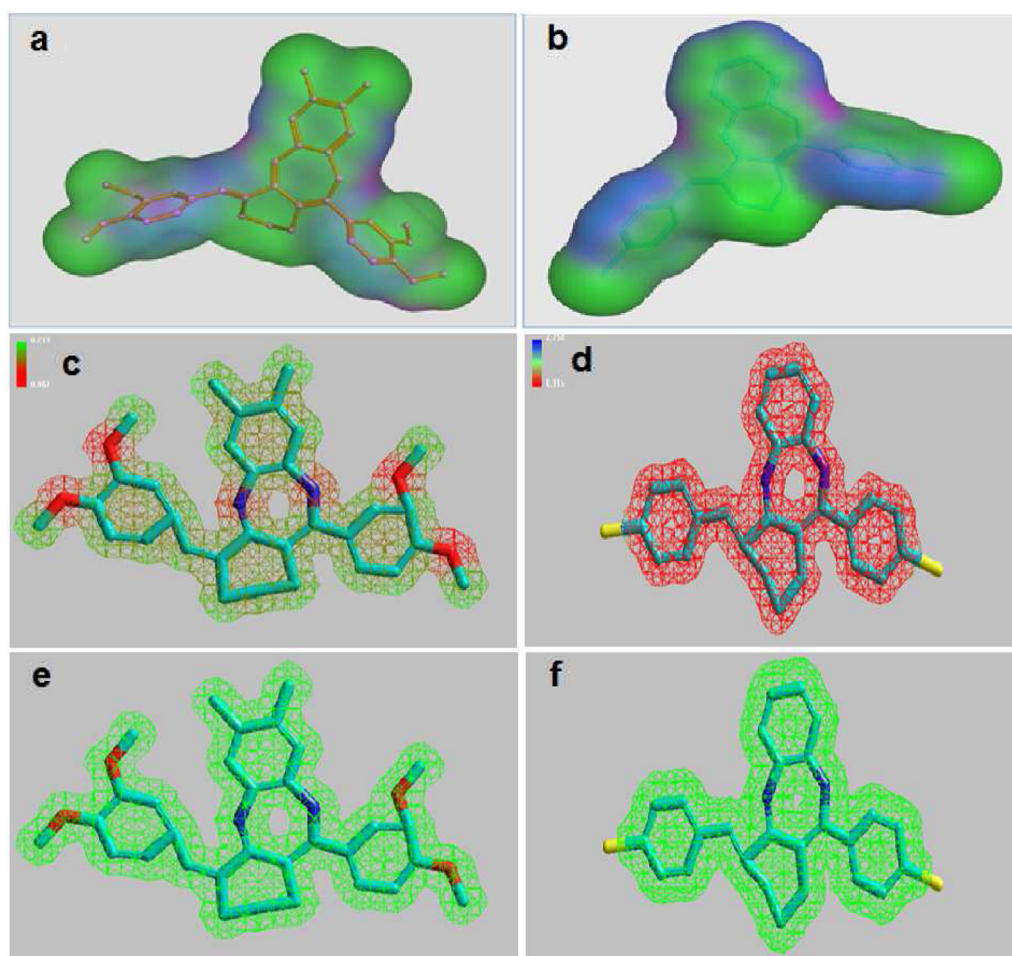


Fig. 5. Surface map for (a) the most active compound **35** (orange); (b) the least active compound **27** (cyan). Pink: hydrogen bond, blue: mild polar, green: hydrophobic region. Electrostatic map of (c) the lowest energy conformers for **35**; (d) the lowest energy conformers for **27**. Red: hydrophilic region, green: hydrophobic region. Total density charge (e) for the most active compound **35**; (f) the least active compound **27**. (For interpretation of the references to color in this figure legend, the reader is referred to the web version of this article.)

proved to be eleven fold more active than 5-FU, with MG-MID GI₅₀, TGI, and LC₅₀ values of 2.0, 12.6, 61.7 μ M, respectively. Structure activity correlation revealed that ring expansion of the tetrahydroquinazolines **16** and **17** produced the dibenzo[b,e][1,4]diazepine derivatives **30** and **31** with remarkable increase in the DHFR inhibition potency at concentrations of 0.06 and 0.09 μ M, respectively. Substitution of the said nuclei with electron donating methoxy function proved to contribute to the magnitude of potency rather than the electron withdrawing halogen atoms. Computer modeling studies allowed the identification of methoxy substituents, the π -system of the chalcone core, N atoms, methyl groups and the dibenzodiazepine ring as pharmacophoric features essential for activity. These mark points could be used as template model for further future optimization.

6. Experimental part

Melting points ($^{\circ}$ C) were determined on Mettler FP80 melting point apparatus and are uncorrected. Microanalyses were performed on a Perkin–Elmer 240 elemental analyzer at the Central Research Laboratory, College of Pharmacy, King Saud University. All of the new compounds were analyzed for C, H and N and agreed with the proposed structures within $\pm 0.4\%$ of the theoretical values. ^1H , ^{13}C NMR spectra were recorded on a Bruker 500 MHz FT spectrometer (the Central Research Laboratory, College of Pharmacy, King Saud University); chemical shifts are expressed in δ ppm with reference to TMS. Mass spectral (MS) data were obtained on a Perkin Elmer, Clarus 600 GC/MS and Joel JMS-AX 500 mass spectrometers. Thin layer chromatography was performed on precoated (0.25 mm) silica gel GF₂₅₄ plates (E. Merck, Germany), compounds were detected with 254 nm UV lamp. Silica gel (60–230 mesh) was employed for routine column chromatography separations. All the fine chemicals and reagents used were purchased from Aldrich Chemicals Co, USA. Compounds **7–11**, **19–23** were previously reported [18,33]. DHFR inhibition activity experiments were performed at Pharmacology Department, Faculty of Pharmacy; Future University in Egypt. Bovine liver DHFR enzyme, methotrexate (MTX) was used in the assay (Sigma Chemical Co, USA). Elisa reader SN208125 Bio Tek MQX200, Software program GEN5 wave length 340 nm was used to measure the changes in absorbance. *In vitro* antitumor testing was conducted at the NCI's disease-oriented human cell lines assay facility, Bethesda, MD, USA. Concerning the molecular modeling study, all experiments were conducted with MOE software except electrostatic potential and total density maps were done using Hyperchem 8.05 package from Hypercube running on a PC computer. Enzyme structure, starting coordinate of hDHFR enzyme in tertiary complex with reduced-nicotinamide adenine dinucleotide phosphate (NADPH) and MTX, code ID 1DLS, was obtained from the Protein Data Bank of Brookhaven National Laboratory [37].

6.1. Chemistry

6.1.1. (E)-8-Substituted benzylidene-2-methyl-4-substituted phenyl-5,6,7,8-tetrahydroquinazolines (**13–17**)

A solution of acetamidine HCl (**12**, 0.94 g, 0.01 mol), the appropriate diarylidene compounds (**7–11**, 0.01 mol) in glacial acetic acid (20 ml) was heated under reflux for 20 h. Solvent was evaporated under vacuum; the obtained residue was dissolved in chloroform, washed with water, and the organic layer was separated, dried and evaporated. The obtained solid was recrystallized from ethanol to yield compounds **13–17**. **13**: ^1H NMR (DMSO-*d*₆) δ 1.22 (s, 3H, CH₃), 1.73 (m, 2H, cyclohexane-H), 2.87 (m, 4H, cyclohexane-H), 7.50 (d, 4H, *J* = 8, Ar-H), 7.58 (s, 1H, CH=C), 7.65 (d, 4H, *J* = 8.5, Ar-H), ^{13}C NMR δ 22.2, 23.7, 27.7, 34.2, 121.0, 122.2,

130.7, 131.0, 131.3, 131.5, 132.2, 132.3, 133.7, 134.5, 134.6, 134.9, 135.3, 136.9, 138.4, 139.2, 188.8, 191.7. MS *m/z* (%): 470 (14.2, M⁺). **14**: ^1H NMR (DMSO-*d*₆) δ 1.25 (s, 3H, CH₃), 1.74 (m, 2H, cyclohexane-H), 2.88 (m, 4H, cyclohexane-H), 7.52 (d, 4H, *J* = 8.5, Ar-H), 7.57 (s, 1H, CH=C), 7.59 (d, 4H, *J* = 8.5, Ar-H), ^{13}C NMR δ 22.2, 23.7, 27.7, 28.0, 34.2, 127.8, 128.6, 131.1, 132.0, 132.1, 132.3, 133.4, 133.5, 133.7, 134.1, 134.5, 134.9, 136.8, 138.4, 139.2, 188.7, 191.6. MS *m/z* (%): 380 (20.2, M⁺). **15**: ^1H NMR (DMSO-*d*₆) δ 1.24 (s, 3H, CH₃), 1.73 (m, 2H, cyclohexane-H), 2.89 (m, 4H, cyclohexane-H), 3.82 (s, 6H, OCH₃), 7.02 (d, 4H, *J* = 8.5, Ar-H), 7.53 (d, 4H, *J* = 9, Ar-H), 7.59 (s, 1H, CH=C). ^{13}C NMR δ 22.5, 24.0, 27.9, 28.2, 34.7, 55.2, 55.4, 113.2, 114.1, 127.9, 128.3, 130.4, 131.5, 132.2, 133.8, 134.2, 134.8, 135.8, 136.2, 136.5, 138.0, 159.7, 188.6, 191.9. MS *m/z* (%): 372 (12.4, M⁺). **16**: ^1H NMR (DMSO-*d*₆) δ 1.21 (s, 3H, CH₃), 1.74 (m, 2H, cyclohexane-H), 2.92 (m, 4H, cyclohexane-H), 3.81 (s, 12H, OCH₃), 7.05 (d, 4H, *J* = 8.5, Ar-H), 7.15 (s, 2H, Ar-H), 7.60 (s, 1H, CH=C). ^{13}C NMR δ 22.4, 24.0, 27.8, 28.2, 34.9, 55.4, 55.5, 56.1, 56.3, 110.9, 111.5, 113.5, 114.1, 123.7, 128.3, 134.3, 135.6, 136.3, 136.8, 147.7, 148.5, 149.1, 149.4, 149.5, 188.5, 191.8. MS *m/z* (%): 432 (5.8, M⁺). **17**: ^1H NMR (DMSO-*d*₆) δ 1.25 (s, 3H, CH₃), 1.75 (m, 2H, cyclohexane-H), 2.96 (m, 4H, cyclohexane-H), 3.83 (s, 18H, OCH₃), 6.87 (s, 2H, Ar-H), 7.60 (s, 1H, CH=C). MS *m/z* (%): 492 (11.9, M⁺).

6.1.2. (4E,4aZ,11Z)-4-(Substituted benzylidene)-11-(substituted phenyl)-2,3,4,10-tetrahydro-1H-dibenzo[b,e][1,4]diazepines (**27–31**)

A solution of 1,2-diaminobenzene (**24**, 1.08 g, 0.01 mol), the appropriate α,β -unsaturated ketone (**7–11**, 0.01 mol) in glacial acetic acid (20 ml) was heated under reflux for 20 h, and continued as mentioned under compounds **13–17**. **27**: ^1H NMR (DMSO-*d*₆) δ 1.73 (m, 2H, cyclohexane-H), 2.87 (m, 4H, cyclohexane-H), 6.72 (brs, 1H, NH), 7.39 (d, 2H, *J* = 8, Ar-H), 7.49–7.51 (m, 6H, Ar-H), 7.58 (s, 1H, CH=C), 7.65 (d, 4H, *J* = 8, Ar-H). ^{13}C NMR δ 2.5, 22.2, 23.7, 27.7, 28.0, 34.2, 62.9, 122.2, 130.7, 130.9, 131.1, 131.3, 131.5, 132.3, 132.8, 133.7, 134.5, 134.6, 134.9, 136.9, 137.1, 138.2, 138.5, 139.0, 188.8, 191.4. MS *m/z* (%): 520 (9.4, M⁺). **28**: ^1H NMR (DMSO-*d*₆) δ 1.73 (m, 2H, cyclohexane-H), 2.88 (m, 4H, cyclohexane-H), 6.76 (brs, 1H, NH), 7.36 (d, 2H, *J* = 8, Ar-H), 7.51–7.53 (m, 6H, Ar-H), 7.57 (s, 1H, CH=C), 7.60 (d, 4H, *J* = 8, Ar-H). MS *m/z* (%): 430 (12.7, M⁺). **29**: ^1H NMR (DMSO-*d*₆) δ 1.73 (m, 2H, cyclohexane-H), 2.89 (m, 4H, cyclohexane-H), 3.80 (s, 6H, OCH₃), 6.76 (brs, 1H, NH), 6.88 (d, 2H, *J* = 8, Ar-H), 7.03 (d, 4H, *J* = 8.5, Ar-H), 7.54–7.52 (m, 6H, Ar-H), 7.57 (s, 1H, CH=C). ^{13}C NMR δ 22.5, 23.9, 27.9, 28.2, 34.7, 38.9, 55.1, 55.3, 113.2, 114.1, 127.9, 128.0, 128.6, 129.5, 129.8, 130.4, 131.5, 132.0, 132.2, 133.1, 134.2, 134.8, 135.4, 136.2, 137.5, 159.7, 188.6, 191.2. MS *m/z* (%): 422 (3.0, M⁺). **30**: ^1H NMR (DMSO-*d*₆) δ 1.75 (m, 2H, cyclohexane-H), 2.92 (m, 4H, cyclohexane-H), 3.78 (s, 12H, OCH₃), 6.65 (brs, 1H, NH), 6.92 (d, 2H, *J* = 8, Ar-H), 7.04 (d, 2H, *J* = 7.5, Ar-H), 7.11–7.19 (m, 4H, Ar-H), 7.40 (s, 2H, Ar-H), 7.60 (s, 1H, CH=C). ^{13}C NMR δ 22.5, 24.0, 27.9, 28.2, 34.9, 38.8, 55.4, 55.5, 61.0, 62.9, 110.9, 111.5, 113.4, 114.0, 123.6, 123.8, 128.2, 128.4, 134.3, 135.1, 135.7, 135.9, 136.3, 137.4, 147.7, 148.4, 149.1, 149.5, 188.6, 191.5. MS *m/z* (%): 482 (18.5, M⁺). **31**: ^1H NMR (DMSO-*d*₆) δ 1.86 (m, 2H, cyclohexane-H), 2.95 (m, 4H, cyclohexane-H), 3.81 (s, 18H, OCH₃), 6.68 (brs, 1H, NH), 6.80 (s, 2H, Ar-H), 6.87 (s, 2H, Ar-H), 6.97 (s, 2H, Ar-H), 7.36 (s, 2H, Ar-H), 7.60 (s, 1H, CH=C). MS *m/z* (%): 542 (30.4, M⁺).

6.1.3. (4E,4aZ,11Z)-7,8-Dimethyl-4-(substituted benzylidene)-11-(substituted phenyl)-2,3,4,10-tetrahydro-1H-dibenzo[b,e][1,4]diazepines (**32–36**)

A solution of 1,2-diamino-4,5-dimethylbenzene (**25**, 1.36 g, 0.01 mol), the appropriate α,β -unsaturated ketone (**7–11**, 0.01 mol) in glacial acetic acid (20 ml) was heated under reflux for 20 h, and continued as mentioned under compounds **13–17**. **32**: ^1H NMR (DMSO-*d*₆) δ 1.69 (s, 6H, CH₃), 1.71 (m, 2H, cyclohexane-H), 2.87 (m, 4H, cyclohexane-H), 6.75 (brs, 1H, NH), 7.32 (s, 1H, Ar-H), 7.41

(s, 1H, Ar–H), 7.49 (d, 4H, $J = 8$, Ar–H), 7.57 (s, 1H, CH=C), 7.65 (d, 4H, $J = 8.5$, Ar–H). MS m/z (%): 548 (10.2, M^+). **33**: ^1H NMR (DMSO- d_6) δ 1.68 (s, 6H, CH_3), 1.75 (m, 2H, cyclohexane–H), 2.87 (m, 4H, cyclohexane–H), 6.74 (brs, 1H, NH), 7.38 (s, 1H, Ar–H), 7.50 (s, 1H, Ar–H), 7.53 (d, 4H, $J = 8.5$, Ar–H), 7.57 (s, 1H, CH=C), 7.58 (d, 4H, $J = 8.5$, Ar–H). ^{13}C NMR δ 22.2, 23.7, 27.7, 28.0, 34.2, 38.8, 62.9, 127.8, 128.5, 128.9, 130.5, 131.0, 131.9, 132.0, 132.1, 132.3, 133.5, 133.6, 134.1, 134.5, 134.8, 134.9, 136.8, 138.1, 138.4, 139.2, 188.8, 191.5. MS m/z (%): 458 (5.2, M^+). **34**: ^1H NMR (DMSO- d_6) δ 1.68 (s, 6H, CH_3), 1.76 (m, 2H, cyclohexane–H), 2.89 (m, 4H, cyclohexane–H), 3.82 (s, 6H, OCH_3), 6.65 (brs, 1H, NH), 6.82 (s, 1H, Ar–H), 7.02 (d, 4H, $J = 8.5$, Ar–H), 7.39 (s, 1H, Ar–H), 7.52 (d, 4H, $J = 8.5$, Ar–H), 7.60 (s, 1H, CH=C). MS m/z (%): 450 (11.2, M^+). **35**: ^1H NMR (DMSO- d_6) δ 1.70 (s, 6H, CH_3), 1.76 (m, 2H, cyclohexane–H), 2.92 (m, 4H, cyclohexane–H), 3.82 (s, 12 H, OCH_3), 6.65 (brs, 1H, NH), 6.91 (s, 1H, Ar–H), 7.04 (d, 2H, $J = 8.5$, Ar–H), 7.39 (m, 4H, Ar–H), 7.40 (s, 1H, Ar–H), 7.60 (s, 1H, CH=C). ^{13}C NMR δ 22.5, 24.0, 27.9, 28.2, 34.9, 38.8, 55.4, 55.5, 59.1, 61.2, 110.9, 111.5, 113.4, 114.0, 120.1, 122.9, 123.7, 123.8, 128.1, 128.4, 134.3, 135.1, 135.7, 135.9, 136.3, 136.9, 147.7, 148.4, 149.1, 149.5, 188.6, 191.9. MS m/z (%): 510 (19.4, M^+). **36**: ^1H NMR (DMSO- d_6) δ 1.86 (s, 6H, CH_3), 2.72 (m, 2H, cyclohexane–H), 2.95 (m, 4H, cyclohexane–H), 3.83 (s, 18 H, OCH_3), 6.69 (brs, 1H, NH), 6.81 (s, 2H, Ar–H), 6.87 (s, 2H, Ar–H), 6.97 (s, 2H, Ar–H), 7.60 (s, 1H, CH=C). MS m/z (%): 570 (24.1, M^+).

6.1.4. (4*E*,4*aZ*,11*Z*)-7,8-Dichloro-4-(substituted benzylidene)-11-(substituted phenyl)-2,3,4,10-tetrahydro-1*H*-dibenzo[*b,e*][1,4]diazepines (**37–41**)

A solution of 1,2-diamino-4,5-dichlorobenzene (**26**, 1.75 g, 0.01 mol), the appropriate α,β -unsaturated ketone (**7–11**, 0.01 mol) in glacial acetic acid (20 ml) was heated under reflux for 20 h, and continued as mentioned under compounds **13–17**. **37**: ^1H NMR (DMSO- d_6) δ 1.73 (m, 2H, cyclohexane–H), 2.87 (m, 4H, cyclohexane–H), 6.74 (brs, 1H, NH), 7.32 (s, 1H, Ar–H), 7.39 (s, 1H, Ar–H), 7.49 (d, 4H, $J = 8$, Ar–H), 7.57 (s, 1H, CH=C), 7.65 (d, 4H, $J = 8.5$, Ar–H). ^{13}C NMR δ 22.2, 23.7, 27.7, 28.0, 34.1, 38.6, 62.9, 122.2, 123.4, 123.9, 124.0, 130.7, 131.3, 131.5, 132.3, 133.7, 134.5, 134.9, 135.2, 136.5, 136.9, 138.4, 138.8, 139.2, 188.8, 191.4. MS m/z (%): 588 (6.3, M^+). **38**: ^1H NMR (DMSO- d_6) δ 1.73 (m, 2H, cyclohexane–H), 2.88 (m, 4H, cyclohexane–H), 6.74 (brs, 1H, NH), 7.37 (s, 1H, Ar–H), 7.47 (s, 1H, Ar–H), 7.49 (d, 4H, $J = 8$, Ar–H), 7.53 (s, 1H, CH=C), 7.59 (d, 4H, $J = 8$, Ar–H). ^{13}C NMR δ 22.1, 23.7, 27.7, 28.0, 34.2, 38.4, 61.0, 123.0, 124.8, 127.7, 127.9, 128.6, 129.5, 131.0, 131.9, 132.1, 133.4, 134.1, 134.4, 134.9, 135.7, 136.8, 137.5, 139.2, 188.7, 191.5. MS m/z (%): 500 (13.0, M^+). **39**: ^1H NMR (DMSO- d_6) δ 1.73 (m, 2H, cyclohexane–H), 2.88 (m, 4H, cyclohexane–H), 3.80 (s, 6H, OCH_3), 6.74 (brs, 1H, NH), 6.89 (s, 1H, Ar–H), 7.03 (d, 4H, $J = 8.5$, Ar–H), 7.41 (s, 1H, Ar–H), 7.53 (d, 4H, $J = 8.5$, Ar–H), 7.60 (s, 1H, CH=C). MS m/z (%): 490 (2.2, M^+). **40**: ^1H NMR (DMSO- d_6) δ 1.75 (m, 2H, cyclohexane–H), 2.91 (m, 4H, cyclohexane–H), 3.80 (s, 12 H, OCH_3), 6.74 (brs, 1H, NH), 6.93 (s, 1H, Ar–H), 7.04 (d, 4H, $J = 8.5$, Ar–H), 7.15 (s, 1H, Ar–H), 7.42 (s, 2H, Ar–H), 7.60 (s, 1H, CH=C). ^{13}C NMR δ 22.5, 24.1, 27.9, 28.2, 34.9, 38.9, 55.4, 55.6, 59.2, 60.4, 110.9, 111.5, 113.4, 114.1, 122.2, 123.7, 124.1, 125.8, 128.1, 130.4, 134.3, 135.1, 135.6, 135.9, 136.3, 136.8, 148.4, 149.5, 188.5, 191.5. MS m/z (%): 550 (14.6, M^+). **41**: ^1H NMR (DMSO- d_6) δ 1.72 (m, 2H, cyclohexane–H), 2.95 (m, 4H, cyclohexane–H), 3.83 (s, 18 H, OCH_3), 6.63 (brs, 1H, NH), 6.75 (s, 1H, Ar–H), 6.85 (s, 1H, Ar–H), 6.97 (s, 2H, Ar–H), 7.52 (s, 2H, Ar–H), 7.67 (s, 1H, CH=C). MS m/z (%): 610 (10.3, M^+).

6.2. Dihydrofolate reductase (DHFR) inhibition assay

The assay mixture contained 0.5 mol/l Tris buffer (A), pH 7.5 and 0.05 mol/l Tris buffer (B), pH 7.5. Stock solutions of FH_2 (25 mg in 1.5 ml of 2-mercaptoethanol and 6.0 ml of buffer A in 0.25 ml

aliquots), NADPH (50 mg in 10 ml of buffer (A) in 0.4 ml aliquots), and DHFR (2.1 U in 10 ml of buffer (B) in 0.5 ml aliquots) stored at -70°C . 130 μl FH_2 reaction solutions, 0.25 ml aliquot of FH_2 stock solution in 8.0 ml of buffer B, yielding a final working concentration of 0.104 g/l, was added to each well of the 96-well flat-bottom microplate reader. 20 μl MTX calibrators or unknown samples and blank of different concentrations 10^{-11} to 10^{-5} (adjusted by DMSO) were added into duplicate wells. The microplate was shaken in a shaking incubator for 1 min, after which 50 μl NADPH/DHFR reaction solution, 0.4-ml aliquot of NADPH stock solution and 0.5 ml aliquot of DHFR stock solution in 6.0 ml of buffer B, yielding a final working concentration of 0.29 g NADPH/l and 15u DHFR/l was added to each well, and the microplate was again shaken in a shaking incubator for 1 min. The absorbance of each well was read in the microplate reader at room temperature at wavelengths of 340 nm [34–36], using the kinetic mode with a reading interval of 1 min for duration of 10 min. The changes in absorbance were downloaded directly into an ELISA reader SN208125 Bio Tek MQX200 computer and analyzed with software Gen5 wave length 340 nm. Results are reported as % inhibition of enzymatic activity calculated using the following formula:

$$\% \text{ Inhibition} = \left(1 - \frac{\Delta A/\text{min}_{\text{test}}}{\Delta A/\text{min}_{\text{DMSO}}} \right) \times 100$$

The linear decrease of absorbance ($\Delta A/\text{min}$) between 0 and 10 min for each MTX or sample was calculated and presented by % of inhibition then plotted against their concentrations (log scale) to obtain a calibration curve [36]. The 50% inhibitory concentration (IC_{50}) of each compound was obtained.

6.3. Antitumor screening

Under a sterile condition, cell lines were grown in RPMI 1640 media (Gibco, NY, USA) supplemented with 10% fetal bovine serum (Biocell, CA, USA), 5×10^5 cell/ml was used to test the growth inhibition activity of the synthesized compounds. The concentrations of the compounds ranging from 0.01 to 100 μM were prepared in phosphate buffer saline. Each compound was initially solubilized in dimethyl sulfoxide (DMSO), however, each final dilution contained less than 1% DMSO. Solutions of different concentrations (0.2 ml) were pipetted into separate well of a microtiter tray in duplicate. Cell culture (1.8 ml) containing a cell population of 6×10^4 cells/ml was pipetted into each well. Controls, containing only phosphate buffer saline and DMSO at identical dilutions, were also prepared in the same manner. These cultures were incubated in a humidified incubator at 37°C . The incubator was supplied with 5% CO_2 atmosphere. After 48 h, cells in each well were diluted 10 times with saline and counted by using a coulter counter. The counts were corrected for the dilution [29–32].

6.4. Docking and molecular modeling study

The three-dimensional structures of the substituted dibenzodiazepine chalcone derivatives, which presented best and worst biological profiles, in their neutral forms were constructed using the MOE of Chemical Computing Group Inc software. Lowest energy conformer of each new analog 'global-minima' was docked into the hDHFR enzyme-binding domain. Enzyme structure. Starting coordinate of hDHFR enzyme in tertiary complex with reduced-nicotinamide adenine dinucleotide phosphate (NADPH) and MTX, code ID 1DLS, was obtained from the Protein Data Bank of Brookhaven National Laboratory [37]. All of the hydrogens were added and enzyme structure was subjected to refinement protocol in which the constraints on the enzyme were gradually removed and

minimized until the rms gradient was 0.01 kcal/mol Å. The energy minimization was carried out using the molecular mechanics force field 'AMBER.' The energy-minimized structure was used for molecular modeling studies keeping all the heavy atoms fixed until an RMSD gradient of 0.05 kcal/mol Å was reached. Ligand structures were built with MOE and minimized using the MMFF94x force field until an RMSD gradient of 0.05 kcal/mol Å was reached. For each of chalcone analog, energy minimizations (EM) were performed using 1000 steps of steepest descent, followed by conjugate gradient minimization to an RMS energy gradient of 0.01 kcal/mol Å. The active site of the enzyme was defined using a radius of 10.0 Å around MTX. Energy of binding was calculated as the difference between the energy of the complex and individual energies of the enzyme and ligand [43,44,47,48]. The docking was performed using the Alpha Triangle placement method and the London dG scoring method. 300 results for each ligand were generated, discarding the results with an RMSD value >3 Å. The best scored result of the remaining conformations for each ligand was further analyzed. The protein/ligand complexes were minimized using the MMFF94x force field, until an RMSD gradient 0.1 kcal/mol/Å° was reached.

6.5. Flexible alignment and superposition

The investigated compounds were subjected to flexible alignment and superposition experiments using 'Molecular Operating Environment' software (MOE of Chemical Computing Group Inc., on a Core 2 duo 2.3 GHz workstation). The molecules were built using the Builder module of MOE. Their geometry was optimized by using the MMFF94 force field followed by a flexible alignment using systematic conformational search. Lowest energy aligned conformation(s) were identified [43,44,47,48].

6.6. Electrostatic potential isosurface maps

Molecular structure of the selected synthesized chalcones was constructed from fragment libraries in the Hyperchem program [49]. The partial atomic charges for each analog were assigned with the semiempirical mechanical calculation method 'AM1' [50,51] implemented in Hyperchem 8.05. Conformational search was formed around all the rotatable bonds with an increment of 10° using conformational search module as implemented in HyperChem 6.03. All the conformers were minimized until the rms deviation was 0.01 kcal/mol Å.

Acknowledgments

The authors extend their appreciation to the Deanship of Scientific Research at King Saud University for funding this work through the research grant number NFG2-08-33.

Appendix A. Supplementary material

Supplementary data related to this article can be found online at <http://dx.doi.org/10.1016/j.ejmech.2014.01.004>.

References

- [1] H. Masur, Problems in the management of opportunistic infections in patients infected with human immunodeficiency virus, *J. Infect. Dis.* 161 (1990) 858–864.
- [2] E.M. Berman, L.M. Werbel, The renewed potential for folate antagonists in contemporary cancer chemotherapy, *J. Med. Chem.* 34 (1991) 479–485.
- [3] N. Gonen, Y.G. Assaraf, Antifolates in cancer therapy: structure, activity and mechanisms of drug resistance, *Drug Resist. Updates* 15 (2012) 183–210.
- [4] P. Borst, M. Quellet, New mechanism of drug resistance in parasitic protozoa, *Annu. Rev. Microbiol.* 49 (1995) 427–460.
- [5] M.F. Mullarkey, B.A. Blumenstein, W.P. Andrade, G.A. Bailey, I. Olason, C.E. Weizel, Methotrexate in the treatment of corticosteroid-dependent asthma. A double-blind crossover study, *N. Engl. J. Med.* 318 (1988) 603–607.
- [6] E.F. Elslager, J.L. Johnson, L.M. Werbel, Folate antagonists 20. Synthesis, antitumor, and antimalarial properties of trimetrexate and related 6-[(phenylamino)methyl]2,4-quinazolin-diamines, *J. Med. Chem.* 26 (1983) 1753–1760.
- [7] E.M. Grivsky, S. Lee, C.W. Sigel, D.S. Duch, C.A. Nichol, Synthesis and antitumor activity of 2,4-diamino-6-(2,5-dimethoxybenzyl)-5-methyl[2,3-d] pyrimidine, *J. Med. Chem.* 23 (1980) 327–329.
- [8] V. Bavetsias, A.L. Jackman, J.H. Marriott, R. Kimbell, W. Gibson, F.T. Boyle, G.M. Bisset, Folate-based inhibitors of thymidylate synthase, *J. Med. Chem.* 40 (1997) 1495–1510.
- [9] V. Bavetsias, J.H. Marriott, C. Melin, R. Kimbell, Z.S. Matusiak, F.T. Boyle, A.L. Jackman, Design and synthesis of cyclopenta[g]quinazoline-based antifolate as inhibitors of thymidylate synthase and potential antitumor agents, *J. Med. Chem.* 43 (2000) 1910–1926.
- [10] C. Sheng-Li, F. Yu-Ping, J. Yu-Yang, L. Shi-Ying, D. Guo-Yu, L. Run-tao, Synthesis and *in vitro* antitumor activity of 4(3H)-quinazolinone derivatives with dithiocarbamate side chains, *Bioorg. Med. Chem. Lett.* 15 (2005) 1915–1917.
- [11] P.C. Wyss, P. Gerber, P.G. Hartman, C. Hubschwerlen, H. Locher, H. Marty, M. Stahl, Novel dihydrofolate reductase inhibitors. Structure-based versus diversity-based library design and high-throughput synthesis and screening, *J. Med. Chem.* 46 (2003) 2304–2312.
- [12] K.M. El-Shaieb, A.A. Hassan, A.S. Abdel-Aal, Synthesis of dibenzo[h,e][1,4] diazepine derivatives, *J. Chem. Res.* 35 (2011) 592–594.
- [13] J.R. Dimmock, P. Kumar, A.J. Nazari, N.L. Motaganahalli, T.P. Kowalchuk, M.A. Beazely, J.W. Quail, E.O. Oloo, T.M. Allen, J. Szydłowski, E. Declercq, J. Balzarini, Cytotoxic 2,6-bis-(arylidene)-cyclohexanones and related compounds, *Eur. J. Med. Chem.* 35 (2000) 967–977.
- [14] J.R. Dimmock, M.P. Podmanilayam, G.A. Zello, K.H. Nienaber, T.M. Allen, C.L. Santos, E. Declercq, J. Balzarini, E.K. Manavathu, J.P. Stables, Cytotoxic analogues of 2,6-bis(arylidene) cyclohexanones, *Eur. J. Med. Chem.* 38 (2003) 169–177.
- [15] H.I. El-Subbagh, S.M. Abu-Zaid, M.A. Mahran, F.A. Badria, A.M. Al-Obaid, Synthesis and biological evaluation of certain α,β -unsaturated ketones and their corresponding fused pyridines as antiviral and cytotoxic agents, *J. Med. Chem.* 43 (2000) 2915–2921.
- [16] B.K. Adams, E.M. Ferstl, M.C. Davis, M. Herold, S. Kurtkaya, R.F. Camalier, M.G. Hollingshead, G. Kaur, E.A. Sauville, F.R. Rickles, J.P. Synder, D.C. Liotta, M. Shoji, Synthesis and biological evaluation of novel curcumin analogs as anticancer and antiangiogenesis agents, *Bioorg. Med. Chem.* 12 (2004) 3871–3883.
- [17] S.A.F. Rostom, G.S. Hassan, H.I. Subbagh, Synthesis and biological evaluation of some polymethoxylated fused pyridine ring systems as antitumor agents, *Arch. Pharm. Chem. Life Sci.* 342 (2009) 584–590.
- [18] F.A. Al-Omary, G.S. Hassan, S.M. El-Messery, H.I. El-Subbagh, Substituted thiazoles V. Synthesis and antitumor activity of novel thiazolo[2,3-b]quinazoline and pyrido[4,3-d]thiazolo[3,2-a]pyrimidine analogues, *Eur. J. Med. Chem.* 47 (2012) 65–72.
- [19] S.T. Al-Rashood, I.A. Aboldahab, L.A. Abouzeid, A.A.-M. Abdel-Aziz, M.N. Nagi, S.G. Abdul-hamide, K.M. Yousef, A.M. Al-Obaid, H.I. El-Subbagh, Synthesis, dihydrofolate reductase inhibition, and molecular modeling study of some new 4(3H)-quinazolinone analogues, *Bioorg. Med. Chem.* 14 (2006) 8608–8621.
- [20] F.A.M. Al-Omary, L.A. Abou-zeid, M.N. Nagi, E.E. Habib, A.A.-M. Abdel-Aziz, A.S. El-Azab, S.G. Abdel-Hamide, M.A. Al-Omar, A.M. Al-Obaid, H.I. El-Subbagh, Non-classical antifolates. Part 2: synthesis, biological evaluation, and molecular modeling study of some new 2,6-substituted-quinazolin-4-ones, *Bioorg. Med. Chem.* 18 (2010) 2849–2863.
- [21] F.A.M. Al-Omary, G.S. Hassan, S.M. El-Messery, M.N. Nagi, E.E. Habib, H.I. El-Subbagh, Nonclassical antifolates, part 3: synthesis, biological evaluation and molecular modeling study of some new 2-heteroarylthio-quinazolin-4-ones, *Eur. J. Med. Chem.* 63 (2013) 33–45.
- [22] G.S. Hassan, S.M. El-Messery, F.A.M. Al-Omary, S.T. Al-Rashood, M.I. Shabayek, Y.S. Abulfadl, E.E. Habib, S.M. El-Hallouty, W. Fayad, K.M. Mohamed, B.S. El-Menshaw, H.I. El-Subbagh, Nonclassical antifolates, part 4. 5-(2-aminothiazol-4-yl)-4-phenyl-4H-1,2,4-triazole-3-thiols as a new class of DHFR inhibitors: synthesis, biological evaluation and molecular modeling study, *Eur. J. Med. Chem.* 66 (2013) 135–145.
- [23] H.I. El-Subbagh, W.A. El-Naggar, F.A. Badria, Synthesis and biological testing of 2,4-disubstituted thiazole derivatives as potential antitumor antibiotics, *Med. Chem. Res.* 3 (1994) 503–516.
- [24] H.I. El-Subbagh, A.M. Al-Obaid, 2,4-Disubstituted thiazoles, II. A novel class of antitumor agents, synthesis and biological evaluation, *Eur. J. Med. Chem.* 31 (1996) 1017–1021.
- [25] H.I. El-Subbagh, A.H. Abadi, J. Lehmann, 2,4-Disubstituted thiazoles, III. Synthesis and antitumor activity of ethyl 2-substituted-aminothiazole-4-carboxylate analogs, *Arch. Pharm. Pharm. Med. Chem.* 332 (1999) 137–142.
- [26] H.I. El-Subbagh, I.E. Al-Khawad, E.R. El-Bendary, A.M. Al-Obaid, Substituted thiazoles IV. Synthesis and antitumor activity of new substituted imidazo[2,1-b]thiazole analogs, *Saudi Pharm. J.* 9 (2001) 14–20.
- [27] S.M. El-Messery, G.S. Hassan, F.A. Al-Omary, H.I. El-Subbagh, Substituted thiazoles VI. Synthesis and antitumor activity of new 2-acetamido- and 2 or 3-propanamido-thiazole analogs, *Eur. J. Med. Chem.* 54 (2012) 615–625.
- [28] G.S. Hassan, S.M. El-Messery, F.A. Al-Omary, H.I. El-Subbagh, Substituted thiazoles VII. Synthesis and antitumor activity of certain 2-(substituted

- amino)-4-phenyl-1,3-thiazole analogs, *Bioorg. Med. Chem. Lett.* 22 (2012) 6318–6323.
- [29] M.R. Grever, S.A. Schepartz, B.A. Chabner, The National Cancer Institute cancer drug discovery and development program, *Semin. Oncol.* 19 (1992) 622–638.
- [30] A. Monks, D. Scudiero, P. Skehan, Feasibility of a high flux anticancer drug screen utilizing a derive panel of human tumor cell lines in culture, *J. Natl. Cancer Inst.* 83 (1991) 757–766.
- [31] M.R. Boyd, K.D. Paull, Some practical considerations and applications of the National Cancer Institute *in vitro* anticancer drug discovery screen, *Drug. Rev. Res.* 34 (1995) 91–109.
- [32] P. Skehan, R. Storeng, D. Scudiero, A. Monks, J. McMahon, D. Vistica, J.R. Warren, H. Bokesch, S. Kenney, M.R. Boyd, New colorimetric cytotoxicity assay for anticancer-drug screening, *J. Natl. Cancer Inst.* 82 (1990) 1107–1112.
- [33] N. Singh, S.K. Pandey, N. Anand, R. Dwivedi, S. Singh, S.K. Sinha, V. Chaturvedi, N. Jaiswal, A.K. Srivastava, P. Shah, M.I. Siddiqui, R.P. Tripathi, Synthesis, molecular modeling and bio-evaluation of cycloalkyl fused 2-aminopyrimidines as antitubercular and antidiabetic agents, *Bioorg. Med. Chem. Lett.* 21 (2011) 4404–4408.
- [34] C. Adamson, M. Balis, L. McCully, S. Godwin, G. Poplack, Methotrexate pharmacokinetics following administration of recombinant carboxypeptidase-G₂ in Rhesus monkeys, *J. Clin. Oncol.* 10 (1992) 1359–1364.
- [35] C. Falk, R. Clark, M. Kalman, Enzymatic assay for methotrexate in serum and cerebrospinal fluid, *Clin. Chem.* 22 (1976) 785–788.
- [36] R. Pignatello, G. Sappinatto, V. Sorrenti, L. Vicari, C. Di-Giacomo, A. Vanella, G. Puglisi, Aliphatic α,γ -bis(amides) of methotrexate. Influence of chain length on *in vitro* activity against sensitive and resistant tumour cells, *Pharm. Pharmacol. Commun.* 5 (1999) 299–305.
- [37] M.G. Nordberg, K. Kolmodin, J. Aqvist, S.F. Queener, P. Hallberg, Design, synthesis, and computational affinity prediction of ester soft drugs as inhibitors of dihydrofolate reductase from *Pneumocystis carinii*, *Eur. J. Pharm. Sci.* 22 (2004) 43–53.
- [38] J.R. Appleman, W.A. Beard, T.J. Delcamp, N.J. Prendergast, J.H. Freisheim, R.L. Blakley, Kinetics of the formation and isomerization of methotrexate complexes of recombinant human dihydrofolate reductase, *J. Biol. Chem.* 263 (1988) 10304–10313.
- [39] R.L. Blakley, L. Cocco, Role of isomerization of initial complexes in the binding of inhibitors to dihydrofolate reductase, *Biochemistry* 24 (1985) 4772–4777.
- [40] J.F. Davies, T.J. Delcamp, N.J. Prendergast, V.A. Ashford, J.H. Freisheim, J. Kraut, Crystal structures of recombinant human dihydrofolate reductase complexed with folate and 5-deazafolate, *Biochemistry* 29 (1990) 9467–9479.
- [41] C. Oefner, A. D'Arcy, F.K. Winkle, Crystal structure of human dihydrofolate reductase complexed with folate, *Eur. J. Biochem.* 174 (1988) 377–385.
- [42] J. Stockman, N.R. Nirmala, G. Wagner, T.J. Delcamp, M.T. DeYarman, J.H. Freisheim, Methotrexate binds in a non-productive orientation to human dihydrofolate reductase in solution based on NMR spectroscopy, *FEBS Lett.* 283 (1991) 267–269.
- [43] P. Labute, C. Williams, M. Feher, E. Sourial, J.M. Schmidt, Flexible alignment of small molecules, *J. Med. Chem.* 44 (2001) 1483–1490.
- [44] S. Kearsley, G.M. Smith, An alternative method for the alignment of molecular structures: maximizing electrostatic and steric overlap, *Tetrahedron Comput. Methodol.* 3 (1990) 615–633.
- [45] C.-M. Chu, S. Gao, M.N.V. Sastry, C.-F. Yao, Iodine-catalyzed Michael addition of mercaptans to α,β -unsaturated ketones under solvent-free conditions, *Tetrahedron Lett.* 46 (2005) 4971–4974.
- [46] V. Cody, C.H. Schwalbe, Structural characteristics of antifolate dihydrofolate reductase enzyme interactions, *Crystallogr. Rev.* 12 (2006) 301–333.
- [47] S. Profeta, N.L. Allinger, Molecular mechanics calculations on aliphatic amines, *J. Am. Chem. Soc.* 107 (1985) 1907–1918.
- [48] N.L. Allinger, Conformational analysis. 130. MM2. A hydrocarbon force field utilizing V1 and V2 torsional terms, *J. Am. Chem. Soc.* 99 (1977) 8127–8134.
- [49] Hyperchem: Molecular Modeling System, Hypercube, Inc., Florida, USA, 1999. Release 6.
- [50] W.D. Cornell, P. Cieplak, C.I. Bayly, I.R. Gould, K.M. Merz Jr., D.M. Ferguson, D.C. Spellmeyer, T. Fox, J.W. Caldwell, P.A. Kollman, A second generation forth field for the simulation of proteins and nucleic acids, *J. Am. Chem. Soc.* 117 (1995) 5179–5197.
- [51] M.J.S. Dewar, E.G. Zoebisch, E.F. Healy, J.J.P. Stewart, AM1: a new general purpose quantum mechanical molecular model, *J. Am. Chem. Soc.* 107 (1985) 3902–3909.